VERIZONA PUBLISHER
Publishing Your Ideas

www.verizonaonlinepublishing.com
Vol: 2, Issue: 1

Material Science and Engineering with Advanced Research

Design and Modelling Methodologies of an Efficient and Lightweight Carbon-fiber Reinforced Epoxy Monocoque Chassis, Suitable for an Electric Car

Evangelos Ch. Tsirogiannis[1*], Georgios E. Stavroulakis[2] and Sofoklis S. Makridis[3]

[1]School of Mechanical Engineering, National Technical University of Athens, Athens, GR15780, Greece

[2]School of Production and Management Engineering, Technical University of Crete, Chania, GR73100, Greece

[3]Department of Environmental and Natural Resources Management, University of Patras, Agrinio, GR30100, Greece

***Corresponding author:** Evangelos Ch. Tsirogiannis, Mechanical Engineering, National Technical University of Athens, Athens, GR, Greece; Tel: +306947089008; E mail: vaggelis.tsirogiannis@gmail.com

Article Type: Research, **Submission Date**: 12 December 2016, **Accepted Date:** 9 February 2017, **Published Date:** 20 February 2017.

Citation: Evangelos Ch. Tsirogiannis, Georgios E. Stavroulakis and Sofoklis S. Makridis (2017) Design and Modelling Methodologies of an Efficient and Lightweight Carbon-fiber Reinforced Epoxy Monocoque Chassis, Suitable for an Electric Car. Mater. Sci. Eng. Adv. Res 2(1): 5-12. doi: https://doi.org/10.24218/msear.2017.21.

Abstract

The design of an electric urban car's chassis for the "Shell Eco Marathon" competition takes into account the usage and the type of the vehicle. The most critical factors of designing the new chassis are: the reduction of the weight, improvement of strength and stiffness and reduction of material and manufacturing cost. Towards this direction, a new design approach for a lightweight carbon-fiber reinforced epoxy (CFRE) monocoque chassis, is proposed, which conforms to structural, ergonomic and aesthetic requirements. For the development of this innovative approach, the parametric design method was chosen, in order for the design to be modified easily. The chassis efficiency, in terms of high strength in low mass, was obtained by following appropriate design steps and rules which conform to the vehicle structural and dynamical constraints and by choosing the composite material CFRE. Additionally, a method that calculates the mechanical properties of the composite material CFRE is presented. Furthermore, a model has been created, which calculates automatically the total loads applied on the vehicle's chassis. Worst case stress scenario was chosen and the model's output was evaluated for the new chassis design.

Keywords: Parametric design, Lightweighting, Chassis, Composites, Carbon-fiber, CFRE, Monocoque, CAD, CAE, Vehicle dynamics, FEM, Modelling, Electric car, Racing, COG, Shell eco marathon, Efficiency, Chassis design, Stress scenario.

Introduction

The main goal of this publication is to demonstrate a strategy plan concerning the designing process and guidelines, the materials, the worst case stress scenario and the loads, for the maximization of the car structure efficiency, in terms of high strength and performance in low mass [1]. By applying the new strategy plan, the chassis of an electric car can have less weight and become more durable. Historically, the studied prototype of the electric car has been employing an aluminium space frame and has already won four trophies in six years, in the Shell Eco Marathon, being placed among the best cars in this European competition.

However, using aluminium as structural material, additional aluminium was required to meet stiffness and strength demands. Furthermore, with the use of space frame as chassis type, there was not enough space to install mechanical and electrical parts. Accordingly, it is necessary to create extra housings on the chassis in order to fit in the mechanical and electrical parts. Moreover, space frame is difficult to be manufactured because it is made out of many parts that are assembled together.

Consequently, according to the strategy plan, a CFRE monocoque chassis design, is proposed, that offers great design freedom and is lighter, stiffer, stronger, easier to manufacture and more spacious than the previous one. To achieve a high quality design, the design specifications were compromised with the team's targets, the ergonomic and safety issues were evaluated, the structural possibilities and limitations regarding the available materials were taken into account, the structural engineering constraints regarding a lightweight, stiff, strong and easy to manufacture design were investigated and the loads that act on the axles were analyzed and calculated. Simulation and manufacturing procedures were outside the scope of this publication. For the three-dimensional design, the ProEngineer Wildfire 5 software was used.

Ergonomics

The driver can be aided in his performance by ensuring that all controls can be easily reached, he/she has a comfortable seating position and that visibility over the front of the chassis is sufficient [2]. The variables for a good seating position are the vertical and horizontal position of the steering wheel, the horizontal position and angle of the seat with respect to the horizontal, the horizontal and vertical position of the pedal assembly, the height and horizontal position of the dashboard and front roll hoop. Besides being comfortable, the driver must be safe at all times [3]. This mainly involves that many rules are followed in order to design a safe car. Some major regulations of Shell Eco Marathon are the existence of a roll bar that withstands 700 N (applied in all directions) and extends 5 cm around driver's helmet, a bulkhead that secures the driver, a wide and long enough chassis design to protect the driver's body and dimensional demands for the chassis to allow for quick driver egress in case of accidents or fire [4]. These regulations are often with respect to a so called 95th percentile male [5] as shown in Figure 1.

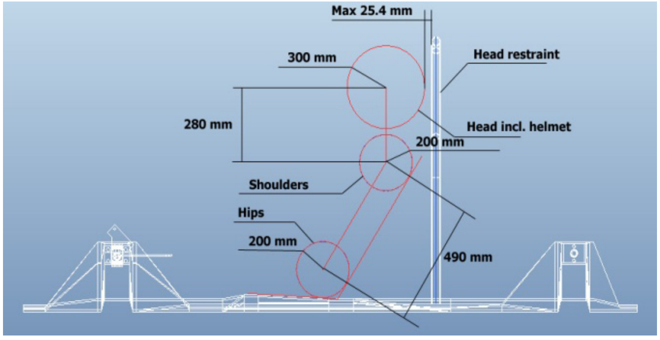

Figure 1: 95th percentile male driver template on our new chassis

New chassis' design

The boundary dimensions of the new chassis design are 1740x730x740 mm. Working with parameters and relations in Pro Engineer, the new chassis design is generated parametrically [6]. It can be updated by changing one or more values of its parameters. To do so, variables and algorithms are used to generate a hierarchy of mathematical and geometric relations [7]. Changing the parameters values, some optimal steps are created for the final design stage of the new chassis as shown in Figure 2.

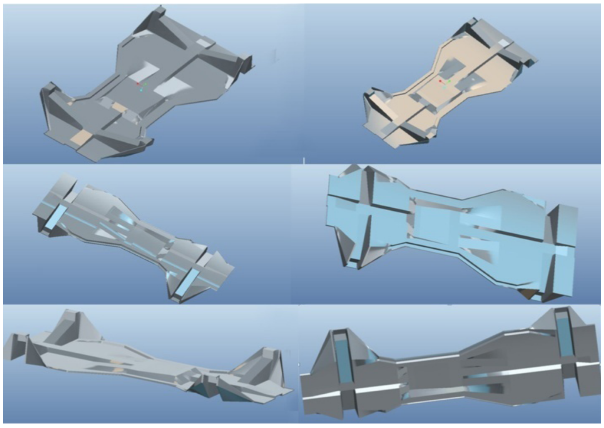

Figure 2: Final design stage

Mechanical properties of the new chassis

The CFRE was chosen as construction material for the principal characteristics strength/light weight, durability, stiffness, fatigue, thermal expansion, energy dampening, corrosion resistance and production flexibility [8,9].

Groups of unidirectional plies cut at various angles from the continuous sheet of "prepreg" are stacked with a sequence that is described by formulae [0/30/0/-15/15/0/-30/0] – 8 plies arranged. Unidirectional pliesmeans that a large percentage of the fibers has the same orientation allowing higher specific moduli in the main fiber direction.

The volume fraction of fiber/resin, can be calculated:

$$V_f = (W_f / d_f) / [(W_f / d_f) + (W_m / d_m)] \quad (1)$$

$$V_m = (1-V_f) \quad (2)$$

where d_f is the density of the fiber, d_m is the density of the resin, W_f is the weight of the fiber, and W_m is the weight of the resin.

Assuming that the structure is a simple beam with length L, consisting of fiber and resin that deform together and the deformation is time independent, a method of estimating the stiffness of a unidirectional composite is performed (rule of mixtures).

$$E_c = E_f V_f + E_m (1-V_f) \quad (3)$$

where E_f is the elastic modulus of the fiber, and E_m is the elastic modulus of the epoxy.

Assuming an anisotropic thin composite lamina with the fibers aligned in the x_1 direction, transverse to the x_2 direction and vertically to the x_3 direction, Young's modulus E, shear modulus G and Poisson ratios ν, in all three axes, are required for its characterization [10].

$$E_x = E_f V_f + E_m (1-V_f) \quad (4)$$

$$E_y = E_f E_m / (E_m V_f + E_f (1-V_f)) \quad (5)$$

$$E_z = E_y \quad (6)$$

$$\nu_{xy} = \nu_f V_f + \nu_m (1-V_f) \quad (7)$$

$$\nu_{yz} = (\nu_{xy} E_t) / E_c \quad (8)$$

$$\nu_{xz} = \nu_{xy} \quad (9)$$

$$G_{xy} = G_m G_f / (G_m V_f + G_f (1-V_f)) \quad (10)$$

$$G_{yz} = E_y / (2(1-\nu_{yz})) \quad (11)$$

$$G_{xz} = G_{xy} \quad (12)$$

Respectively, the longitudinal tensile strength, the transverse tensile strength and the compression strength on the composite are listed.

$$\sigma_x = \sigma_f V_f + \sigma_m (1-V_f) \quad (13)$$

$$\sigma_y = \sigma_m (1-\sqrt{(4V_f / \pi)}) \quad (14)$$

$$\sigma_{compx} = G_m / (1-V_f) \quad (15)$$

where σ_f is the fibers stress levels, and σ_m is the resin stress levels.

For the multi-ply laminates, the tensile modulus, the shear modulus and the Poisson ratio of a random continuous-fiber composite can be calculated by:

$$E = (3 / 8) E_1 + (5 / 8) E_2 \quad (16)$$

$$G = (1 / 8) E_1 + (1 / 4) E_2 \quad (17)$$

$$\nu = (E-2G) / 2G \quad (18)$$

where E_1 is the longitudinal modulus, and E_2 is the transverse modulus for a unidirectional lamina.

The Krenchel model is utilized for the approximation of the strengths of multi-ply laminates. The efficiency factor, n_θ, is used in a mixture-rule calculation [11]:

$$n_\theta = \sum a_n \cos^4 \theta \quad (19)$$

$$\sigma_c = n_\theta \sigma_{fu} V_f + \sigma_m (1-V_f) \quad (20)$$

Table 1 and Table 2 provides the properties of unidirectional CFRE and multi-ply laminates.

Table 1: Properties of unidirectional CFRE

	VALUE	UNIT
Elastic modulus Ex	380.100	Gpa
Elastic modulus Ey	28.269	Gpa
Elastic modulus Ez	28.269	Gpa
Poisson ratio vxy	0.336	
Poisson ratio vyz	0.025	
Poisson ratio vxz	0.336	
Shear modulus Gxy	4.213	Gpa
Shear modulus Gyz	13.790	Gpa
Shear modulus Gxz	4.213	Gpa
Tensile strength σx	2539.400	Mpa
Tensile strength σy	8.251	Mpa
Compressive strength σcompx	4.722	Gpa

Table 2: Properties of multi-ply laminates

PROPERTIES	VALUE	UNIT
Elastic modulus E	160.206	Gpa
Shear modulus G	54.580	Gpa
Tensile strength σ_c	971.400	Mpa
Poisson ratio v	0.468	

Mass and center of gravity definition

Pro Engineer gives that the new chassis mass value is 5.38 kg. Thus, the total vehicle's weight (with the driver on seat) is 149.64 kg. It can also provide the center of gravity of the chassis. Thereafter, the different centers of gravity (battery light, steering system, driver+seat, chassis, fuel cell, electric motor) are added up, and form the main center of gravity [12-16] as shown in Table 3.

Table 3: New vehicle's center of gravity

COGx (mm)	COGy (mm)	COGz (mm)
867.900	391.178	419.625

Determine the worst case stress scenario

The loads of a chassis structure are divided into crash, ride, towing, aerodynamic, cornering, braking and tractive loads. Crash cases are often the most difficult and critical to design. These are outside the scope of this publication, since the structure moves out of the elastic regime into deep collapse. The ride loads is one of the more important criteria by which people judge the design and construction "quality" of a car. However, in this case, the track road is not rough, but quite smooth [17]. Towing loads cannot be neglected, but the vehicle will not need to tow another vehicle. Aerodynamic loads also stress the vehicle structure. Nevertheless, these loads are negligible because the forward velocity is very small (20 km/h – 30 km/h). Consequently, static, cornering and braking loads were taken into account.

Cornering loads are maximized when the vehicle's speed is at maximum speed and its turning radius is minimized. At the Shell Eco Marathon's track, in Rotterdam, there are four counterclockwise andone clockwise turns with approximately the same angle (90°). Regarding to the driving strategy the vehicle runs at high speed (30km/h) on first turn [18]. Therefore, the first turn has been investigated while the chosen racing line depends on the characteristics of the car, the cornering strategies and the conditions around. In the apex point of the corner, the maximum speed and stress is reached. So, the apex of the first turn is the point where there is the cornering worst case stress scenario.

Braking loads cause larger loads than tractive loads [19]. Thus, a real situation needs to be considered when the chassis is overloaded during braking. Supposing that while the vehicle moving on the track,with its maximum speed, 30 km per hour, the preceding vehicle suddenly brakes. Therefore, the driver is forced to brake immediately, to avoid the collision. At this point, it is needed to find a realistic "deceleration scenario" for urban cars, to determine the deceleration value. The "Autonomous Emergency Braking" (AEB) test of Euro NCAP is chosen. Randomly, the Fiat's braking control system is selected to see how it behaves in braking tests [20]. At speeds between 20 km/h and 30 km/h, the brakes apply a maximum deceleration of 6 m/s^2. In our case it is also supposed, that the driver'sreflexes during braking, are as good as Fiat's braking control system. Thus, the vehicle will be subjected tobrake with a deceleration equal to 6 m/s^2 from 30 km/h to 0 km/h [21-23].

In order to demonstrate the strength of the chassis, it only has to be shown that it withstands the total load worst case stress scenario that is the combination of cornering and braking worst case stress scenario. Thus, it is needed to study the scenario where the vehicle is turning in the 1st corner and while is positioned in the apex with 30km/h, it encounters a stationary preceding vehicle and decelerates immediately (6 m/s^2), to avoid the accident.

Dynamic axle loads

Presuming that the vehicle sits statically on level ground, the vertical loads can be calculated [17].

$$W_f = Mg\,(c / L) \tag{27}$$

$$W_r = Mg\,(b / L) \tag{28}$$

where M is the vehicle mass, g is the gravity acceleration, b is the distance from the front axle to the CG, and c is the distance from the rear axle to the CG.

According to the lateral dynamics, the two front wheels can be represented by one wheel at a steer angle δ, with a cornering force equivalent to both wheels. The same assumption is made for the rear wheels[17].

$$F_y = F_{yf} + F_{yr} = (MV^2) / R \tag{29}$$

where V is the forward velocity.

During cornering, a dynamic load transfer from the inside to the outside wheels occurs (the second mechanism for this study is zero, because the chassis has not springs) [24].

$$F_{zo} - F_{zi} = (2F_y\, h_r) / t + (2K_\varphi\, \varphi) / t \tag{30}$$

where, h_r is the roll center height, K_φ is the roll stiffness of the suspension, and φ is the roll angle of the body.

The torque generated by the rotor, for each wheel brake, as well as the total braking force is defined [25-27].

$$\begin{aligned}
&F_{bp} = F_d\,\{L_2 / L_1\} \Rightarrow \\
&P_{mc} = F_{bp} / A_{mc} \Rightarrow \\
&P_{cal} = P_{mc} \Rightarrow \\
&F_{cal} = P_{cal}\, A_{cal} \Rightarrow \\
&F_{clamp} = 2F_{cal} \Rightarrow \\
&F_{friction} = F_{clamp}\, \mu_{bp} \Rightarrow \\
&T_r = F_{friction}\, R_{eff} \Rightarrow \\
&T_t = T_w = T_r \Rightarrow \\
&F_{tire} = T_t / R_t \Rightarrow \\
&F_{total} = \sum F_{(tireLF,RF,LR,RR)}
\end{aligned} \tag{31}$$

where F_{bp} is the force output of the brake pedal, F_d is the force applied to the pedal pad by the driver, L_1 is the distance from the brake pedal arm pivot to the output rod clevis attachment, L_2 is the distance from the brake pedal arm pivot to the brake pedal pad, P_{mc} is the hydraulic pressure by the master cylinder, A_{mc} is the effective area of the master cylinder hydraulic piston, P_{cal} is the hydraulic pressure to the calliper, F_{cal} is the linear mechanical force by the calliper, A_{cal} is the effective area of the calliper hydraulic piston, F_{clamp} is the clamp force by the calliper, $F_{friction}$ is the

Citation: Evangelos Ch. Tsirogiannis, Georgios E. Stavroulakis and Sofoklis S. Makridis (2017) Design and Modelling Methodologies of an Efficient and Lightweight Carbon-fiber Reinforced Epoxy Monocoque Chassis, Suitable for an Electric Car. Mater. Sci. Eng. Adv. Res 2(1): 5-12. doi: https://doi.org/10.24218/msear.2017.21.

frictional force by the brake pads, μ_{bp} is the coefficient of friction between the brake pad and the rotor, T_r is the torque generated by the rotor, R_{eff} is the effective radius of the rotor, T_t is the torque in the tire, T_w is the torque in the wheel, F_{tire} is the force in the tire, and R_t is the effective rolling radius of the loaded tire.

During braking, a dynamic load transfer from the rear to the front axle occurs [25,28].

$$WT = (a_v / g)\times(h_c g / L)\times(M\times g) \quad (32)$$

where a_v is the deceleration, and h_{cg} is the vertical distance from the CG to ground.

Chassis load calculator (CLC) model

The values of the forces acting on a vehicle structure change depending on the characteristics of the structure.

Therefore, for academic and research purposes, a model created which automatically calculates the magnitude and the direction of the loads acting on each vehicle, by importing the characteristics of the vehicle. In order to validate the derived model, data such as track width, wheelbase, center of gravity, mass, et cetera were used as inputs. The breakthrough in this research work is the overcoming of the time consuming process to calculate the corresponding forces of different design structures of the car with the use of CLC model.The equations (27) to (32) that were utilized to implement this model are derived from the theory of Vehicle Dynamics. According to the chosen stress scenario and the imported characteristics of the new chassis, the applied loads are calculated.

First of all, the vertical loads are identified as shown in Table 4 and Table 5.

Table 4: The data used for the calculation of vertical dynamics

Distance from the front axle to the CG	602.900 mm
Distance from the rear axle to the CG	692.100 mm
Distance from the left side of the chassis to the CG	391.178 mm
Distance from the right side of the chassis to the CG	338.822 mm

Table 5: Vertical dynamics

Static load on the left front wheel	372.264 N
Static load on the right front wheel	429.788 N
Static load on the left rear wheel	324.286 N
Static load on the right rear wheel	374.396 N

Then, the lateral loads are calculated according to the cornering worst case stress scenario as presented in Table 6 and Table 7.

Table 6: The data used for the calculation of lateral dynamics

Initial forward velocity	8333 mm/s
Turn radius	10000 mm
Gravity acceleration	9810 mm/s^2
Roll center height	280 mm
Track width	910 mm
Distance of chassis on y axis	730 mm
Track width (-) Distance of chassis on y axis	180 mm
Track width (-) Distance of chassis on y axis (from one side)	90 mm

Table 7: Lateral dynamics

Cornering force	1062.276 N
Load transfer on the right	653.708 N
Load transfer on the left	-653.708 N

During cornering the mass distribution changes, as well as the center of gravity [15,16,29]. Assuming that there is no mass transfer in the z axis, since the car has not shock absorbers as well as the fact that if there is a mass transfer in the x axis, it will be negligible, then the new COGshown in Table 8.

The mass distribution changes during the ¼ turn as given in Table 9.

Table 8: New center of gravity during cornering

COGx (mm)	COGy (mm)	COGz (mm)
867.900	704.022	419.625

Table 9: Mass distribution on left and right wheels

Distribution of mass on the right side	96.441 %
Distribution of mass on the left side	3.559 %

The braking loads are calculated according to the braking worst case stress scenario as presented in Table 10, Table 11, Table 12, Table 13, Table 14, Table 15 and Table 16.

Table 10: Data used for the calculation of braking loads

Final forward velocity	0 mm/s
Absolute value of velocity change	8333 mm/s
Braking time	10 s
Braking distance	83330 mm
Maximum deceleration	833.300 mm/s^2
Wheelbase	1295 mm
Front area of front axle	265 mm
Tyre coefficient of friction	0.0025

Table 11: Data for the brake system dimensions

Distance from the brake pedal arm pivot to the output rod clevis attachment	L1	
Distance from the brake pedal arm pivot to the brake pedal pad	L2	
	Front	**Rear**
Wheel radius	280 mm	280 mm
Master cylinder diameter	12.7mm	12.7 mm
Distance-pushrod to balance bar pivot	30 mm	40 mm
The effective area of the calliper hydraulic piston found on one half of the calliper body	800 mm^2	800 mm^2
Pad coefficient of friction	0.35	0.35
Disc diameter	160 mm	160 mm
Pad depth	3 mm	3 mm
Gap between top of pad and disc	1 mm	1 mm

Table 12: Data for the dynamic characteristics of the vehicle

Cg Height	408.793 mm
Wheelbase	1295 mm
Front wheel rolling radius	280 mm
Rear wheel rolling radius	280 mm
Weight on the front axle	82.309 kg
Weight on the rear axle	72.791 kg
Total weight	155.1 kg
Percentage weight on the front axle	0.531 %
Percentage weight on the rear axle	0.469 %

Table 13: Force applied on the balance bar by the driver

Kgf applied to pedal	10 kgf
Force applied to pedal	98.1 N
Pedal ratio	4:1
Force on balance bar	392.4 N

Table 14: Braking force calculation

	Front	Rear
Balance bar proportion	0.571	0.429
Force on M Cyl piston	224.229 N	168.171 N
Master/cylinder area	126.613 mm^2	126.613 mm^2
Line pressure generated by the master cylinder	1.771 N/mm^2	1.328 N/mm^2
Line hydraulic pressure transmitted to the calliper	1.771 N/mm^2	1.328 N/mm^2
The one sided linear mechanical force generated by the calliper	1416.785 N	1062.588 N
Clapping force on disc generated by the calliper	2833.569 N	2125.177 N
The frictional force generated by the brake pads opposing the rotation of the rotor	991.749 N	743.812 N
Fx=Fsin45	701.273 N	525.955 N
Fy=Fcos45	701.273 N	525.955 N
Disc effective radius	77.5 mm	77.5 mm
Disc torque, the torque generated by the rotor (both pads 1 wheel)	76860.566 Nmm	57645.425 Nmm
The torque found on the tire = torque wheel = torque by the rotor	76860.566 Nmm	57645.425 Nmm
The force reacted between the tire and the ground (assuming friction exists to support the force	274.502 N	205.877 N

Table 15: Deceleration and stopping distance

Total force (4 wheels)	960.757 N
Deceleration a	6194.436 mm/s^2
Stopping distance	5604.940 mm

Table 16: Load transfer from braking

	Front	Rear
Weight transfer	31.735 kg	-31.735 kg
Axle load under braking	113.493 kg	39.487 kg
Dynamic axle load	1113.371 N	387.363 N
Load transfer from braking on the left side	11.079 N	-11.079 N
Load transfer from braking on the right side	300.240 N	-300.240 N

Resulting all the above, a 6.19 m/s^2 deceleration was achieved, whose value is greater than the maximum value of the Fiat's deceleration (6 m/s^2), which was first set as a goal shown in Table 15.

In the case of both braking and turning loads, the mass distribution changes, as well as the center of gravity of the vehicle [15,16,29]. Assuming that there is no mass transfer in the z axis, since the car has not shock absorbers, as well as the fact that if there is a mass transfer in the y axis, it will be negligible, then the new COG shown in Table 17.

Table 17: New center of gravity during braking and cornering

COGx	COGy	COGz
599.260	704.022	419.630

This is the center of mass that the vehicle has during braking and cornering coexistence. It is observed that after such a sudden stop in a ¼ turn the mass distribution changes presented in Table 18.

Table 18: Mass distribution on front and rear axles

Distribution of mass on front axle	74.188 %
Distribution of mass on rear axle	25.812 %

With the new center of mass, the cornering force on each wheel can be found in Table 19.

Table 19: The cornering force on each wheel with the new center of gravity

Cornering force (front)	788.086 N
Cornering force (rear)	274.190 N
Cornering force on the left front wheel	28.045 N
Cornering force on the right front wheel	760.041 N
Cornering force on the left rear wheel	9.757 N
Cornering force on the right rear wheel	264.433 N

Summarizing, the loads that act on each semi-axle of the chassis, in the z axis, are presented in Table 20.

Table 20: Combination load case

Static load on the left front wheel	372.264 N
Static load on the right front wheel	429.788 N
Static load on the left rear wheel	324.286 N
Static load on the right rear wheel	374.396 N
Load transfer from cornering on the right front wheel	484.976 N
Load transfer from cornering on the right rear wheel	168.732 N
Load transfer from cornering on the left front wheel	-484.976 N
Load transfer from cornering on the left rear wheel	-168.732 N
Load transfer from braking on the left front wheel	11.079 N
Load transfer from braking on the right front wheel	300.240 N
Load transfer from braking on the left rear wheel	-11.079 N
Load transfer from braking on the right rear wheel	-300.240 N

E verytotal force applied to each semi-axle, in the upward direction on the z axis and is calculated by the sum of the above loads shown in Table 21.

Table 21: Total dynamic loads on each wheel (z axis)

Total dynamic load on the left front wheel	-101.633 N
Total dynamic load on the left front wheel	1215.004 N
Total dynamic load on the left front wheel	144.475 N
Total dynamic load on the left front wheel	242.888 N

The cornering forces F_y are transferred from the contact patch to the center of the axle. The equivalentsystem will consist ofthe cornering forces (F_y) plus the moments (M_x) that are created from the cornering forces. These moments are the result of the cornering forces multiplied by the vertical distance, which is z=280mm as presented in Table 22.

Table 22: Cornering forces Fy and moments Mx from contact patch to the center of axle

Fy on the left front wheel	28.045 N
Fy on the right front wheel	760.041 N
Fy on the left rear wheel	9.757 N
Fy on the right rear wheel	264.433 N
Mx on the left front axle	7852.662 Nmm
Mx on the right front axle	212811.430 Nmm
Mx on the left rear axle	2732.090 Nmm
Mx on the right rear axle	74041.136 Nmm

Thebrakingforceneeds to be analyzed in x and z axis (F_x, F_z) as shown in Table 23.

Table 23: Braking forces

	Fx	Fz
Braking force on the left front axle	701.273 N	701.273 N
Braking force on the right front axle	701.273 N	701.273 N
Braking force on the left rear axle	525.954 N	525.954 N
Braking force on the right rear axle	525.954 N	525.954 N

The vertical distance of F_z from the end of the axle is calculated as well as the vertical distance of F_x from the center of the axle presented in Table 24.

Table 24: Vertical distances

x=(cos45)*0.0075 + 0.0075	12.803 mm
y=(sin45)*0.0075	5.303 mm

F_x, F_z are transferred to the axle. The equivalentsystem willconsist ofthe braking forces (F_x, F_z) plus the moments (M_{y1}, M_{y2}) that are created from the braking forces as shown in Table 25.

Table 25: Braking forces Fx, Fz and moments My1, My2 from disc effective radius to the axle

Braking forces	**Fx**	**Fz**
Left front axle	701.273 N	701.273 N
Right front axle	701.273 N	701.273 N
Left rear axle	525.954 N	525.954 N
Right rear axle	525.954 N	525.954 N
Moments from braking forces	**My1**	**My2**
Left front axle	3719.060 Nmm	8978.604 Nmm
Right front axle	3719.060 Nmm	8978.604 Nmm
Left rear axle	2789.295 Nmm	6733.953 Nmm
Right rear axle	2789.295 Nmm	6733.953 Nmm

Conclusion

The new chassis is extremely light, only 5.38 kg and consequently less energy is consumed to move it, comparing to the previous one that weights 10.85 kg. This energy decrease is significantly high taking into account that the previous one was the lightest chassis of the competition. Furthermore, the ergonomics and the aesthetic acceptance of the new chassis is better than the previous one.

Consequently, the breakthrough in this research work was not only the achievement of the lightest chassis in the Shell Eco Marathon competition that combines ergonomics, aesthetic and strength demands but also the overcoming of the time consuming process to calculate the corresponding forces of different design structures of the car with the creation and use of the CLC model.

In the future, a FEM model will be developed and used in order to demonstrate the resistance of the new chassis design under the aforementioned extreme stress scenario.

Acknowledgements

Open access fees were covered by the Municipality of Agrinio, Western Greece. Authors are grateful to the Mayor of Agrinio, Mr. George Papanastasiou.

References

1. Budynas-Nisbett. Mechanical Engineering [Internet]. McGraw-Hill; 2006. Available from: www.uotechnology.edu.iq/.../Mechanical Engineering Design.pd...%5Cn.

2. Carello M, Messana A. IDRA pegasus : a fuel-cell prototype for 3000 km/L. Comput Aided Des Appl [Internet]; 2015; 12(sup1):56–66. Available from: http://www.tandfonline.com/doi/full/10.1080/16864360.2015.1077076.

3. Formula SAE Rules [Internet]; 2008. Available from: http://fsaeonline.com.

4. Shell Eco Marathon Official Rules [Internet]; 2014. Available from: http://www.shell.com.

5. Kerkhoven JDG Van. Design of a Formula Student race car chassis. Technische Universiteit Eindhoven; 2008.

6. Pro Engineer User Guide [Internet]; 2008. Available from: http://www.ptc.com.

7. Lee J, Gu N, Jupp J, Sherratt S. Evaluating Creativity in Parametric Design Processes and Products: A Pilot Study. In: Proceedings of Design Computing and Cognition (DCC) [Internet]. Springer; 2012. p. xx-yy. Available from: http://mason.gmu.edu/~jgero/conferences/dcc12/DCC12DigitalProceedings/Digital pdf/Lee.pdf.

8. Hull D, Clyne TW. An introduction to composite materials. Cambridge University.

9. Eurenius CA, Danielsson N, Khokar A, Krane E, Olofsson M, Wass J. Analysis of Composite Chassis. Chalmers University of Technology; 2013.

10. Duleba B, Greskovic F. Simulation of Loading the Polymer / Carbon Fiber Composites and Prediction of Safety Factors. Int J Eng Innov Technol. 2013; 2(8):134–40.

11. Harris B. Engineering composite materials. London: The Institute of Materials; 1999. 261 p.

12. Wagtendonk WJ. Principles of Helicopter Flight. Washington: Aviation Supplies & Academics Inc.; 1996.

13. Seddon J. Basic Helicopter Aerodynamics. Oxford: BSP Professional Books; 1990.

14. Prouty RW. Helicopter Performance Stability and Control. Florida: Krieger Publishing Company; 1990.

15. Hakewill J. Measuring center-of-gravity height on a Formula Car [Internet]; 2007. Available from: www.jameshakewill.com.

16. Baraff D. Physically Based Modeling-Rigid Body Simulation [Internet]; 2001. Available from: http://graphics.cs.cmu.edu/courses/15-869-F08/lec/14/notesg.pdf.

17. Gillespie TD. Fundamentals of Vehicle Dynamics [Internet]. Warrendale: Society of Automotive Engineers, Inc; 1992. 519 p. Available from: http://books.sae.org/book-r-114.

18. Omar SMHS, Arshad NM, Fakharuzi MHAM, Ward TA. Development of an energy efficient driving strategy for a fuel cell vehicle over a fixed distance and average velocity. In: Proceedings - 2013 IEEE Conference on Systems, Process and Control, ICSPC 2013. Kuala Lumpur, Malaysia; 2013. p. 117–20.

19. Jason C. Brown, A. John Robertson STS. Motor Vehicle Structures. Butterworth-Heinemann; 2002.

20. Euroncap [Internet]; 2014. Available from: http://www.euroncap.com/.

21. Schram R, Williams A, Ratingen M van. Implementation of autonomous emergency braking (AEB), the next step in euro NCAP’ s safety assessment. In: The 23rd International Technical Conference on the Enhanced Safety of Vehicles (ESV). Belgium; 2013. 1–6 p.

22. Hulshof W, Knight I, Edwards A, Avery M, Grover C. Autonomous emergency braking test results. In: Proceedings of the 23rd International Technical Conference on the Enhanced Safety of Vehicles (ESV) [Internet]. UK; 2013. 1–13 p. Available from: http://www-nrd.nhtsa.dot.gov/Pdf/ESV/esv23/23ESV-000168.pdf.

23. Sandner V. Development of a test target for AEB systems-Development process of a device to test AEB systems for consumer tests. In: ADAC. Germany; 2006. 1–7 p.

24. Carlos A. Reyes Ruiz, Edgar I. Ramírez Díaz, Osvaldo Ruiz Cervantes, Rafael Schouwenaars AOP. Modeling of the suspension of a passenger bus by finite element software. In: 3rd International Conference on Engineering Optimization. Rio de Janeiro, Brazil; 2012.

25. James Walker J of scR motorsports. The Physics of Braking Systems. StopTech LLC; 2005.

26. Limberg J. Introduction to Foundation Brake Design. E and J Enterprises, Bosch, St. Mary’s College; 2015.

27. Hamilton E, Klang E. Design of Formula SAE Brake Systems. In: Wolfpack Motorsports. Raleigh; 2009.

28. Gritt PS. An Introduction to Brake Systems. In: SAE Brake Colloquium. DaimlerChrysler; 2002. 1–52 p.

29. Bender J, Erleben K, Trinkle J, Coumans E. Interactive Simulation of Rigid Body Dynamics in Computer Graphics. Comput Graph Forum [Internet]. 2014; 33(1):246–70. Available from: http://onlinelibrary.wiley.com/doi/10.1111/cgf.12272/full%5Cnhttp://doi.wiley.com/10.1111/cgf.12272.